v_2 vs p_T in p+Au at RHIC

by

Theodore Koblesky

B.S., University of Illinois, 2011

A thesis submitted to the

Faculty of the Graduate School of the

University of Colorado in partial fulfillment

of the requirements for the degree of

Doctor of Philosophy

Department of Physics

2017

This thesis entitled:
v_2 vs p_T in p+Au at RHIC
written by Theodore Koblesky
has been approved for the Department of Physics

_____

Prof. James Nagle

_____

Prof. Standin

_____

Ms. Standin

Date _____

The final copy of this thesis has been examined by the signatories, and we find that both the content and the form meet acceptable presentation standards of scholarly work in the above mentioned discipline.

Koblesky, Theodore (Ph.D., High Energy Nuclear Physics)

v_2 vs p_T in p+Au at RHIC

Thesis directed by Prof. James Nagle

Abstract

Here is a default abstract. Here is a default abstract. Here is a default abstract. Here is a default abstract. Here is a default abstract. Here is a default abstract. Here is a default abstract. Here is a default abstract. Here is a default abstract. Here is a default abstract. Here is a default abstract. Here is a default abstract. Here is a default abstract. Here is a default abstract. Here is a default abstract. Here is a default abstract. Here is a default abstract. Here is a default abstract. Here is a default abstract.

Dedication

To some of the of the fluffy kitties.

Acknowledgements

People

Contents

Tables

Figures

Chapter 1

Results and Discussion

The v_2 measurement for p+Au$\sqrt{s_{_{NN}}}$= 200 GeV $0-5\%$ centrality completes the set of flow measurements in the small systems available at RHIC: p+Au, d+Au, and ^{3}He+Au. The goal of this set of measurements is to determine the effect of varying initial collision conditions on the resulting flow.

1.1 v_2 Measurement

The resulting v_2 measurement for p+Au $\sqrt{s_{_{NN}}}$= 200 GeV $0-5\%$ centrality is shown in **??**. The systematic uncertainty is very large especially at high p_T and is dominated by non-flow. The fact the non-flow component is so large warrants further discussion.

1.1.1 Non-flow Contribution

As was discussed in section .xxx, the non-flow systematic uncertainty can instead be thought of as a systematic error that can be corrected for in our measurement. To further explore this non-flow effect, Figure **??** shows what the p+Au measurement looks like by subtracting the points off the non-flow uncertainty. Due to non-flow being the dominant source of systematic uncertainty, the corrected p+Au points are at the bottom of the systematic uncertainty boxes of the uncorrected points. The substantial changes this correction makes to the p+Aupoints, especially at high p_T, must be put in context of the field of heavy ion physics. This procedure to estimate the contribution of elementary processes to the measured v_2 signal is an attempt at an accurate approximation. Al-

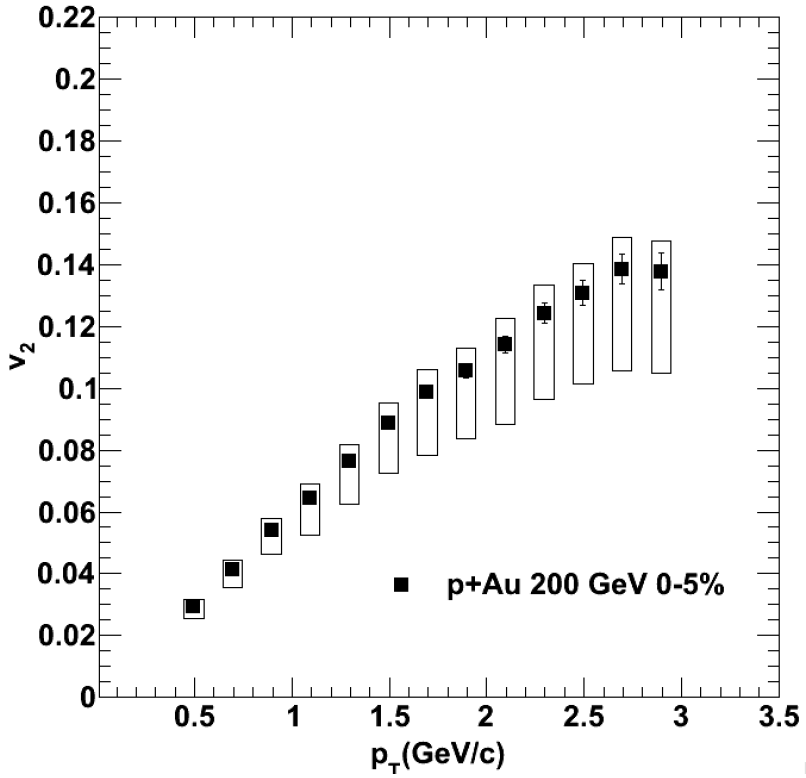

Figure 1.1: The v_2 measurement of p+Au at $\sqrt{s_{NN}}$= 200 GeV 0-5% centrality.

though the non-flow approximation used in this thesis has its merits, there is currently no consensus in the field regarding how to properly quantify how much of the v_2 corresponds to "flow" and how much corresponds to "non-flow." Other experimental collaborations making flow measurements, such as STAR, ATLAS, and ALICE, treat non-flow in different ways **TODO add refs for each collab**. Therefore, we choose to explicitly state our methodology to estimate this non-flow and to treat it as a systematic effect that raises the measured v_2.

1.2 Comparison with Other Species at $\sqrt{s_{NN}}$= 200 GeV 0-5% Centrality

The substantial v_2 p+Au is interesting in itself but the significance of the measurement is best understood by comparing it to other small collision system results, specifically He+Au and d+Au. In order to properly make the strongest physics statement possible in this comparison, we

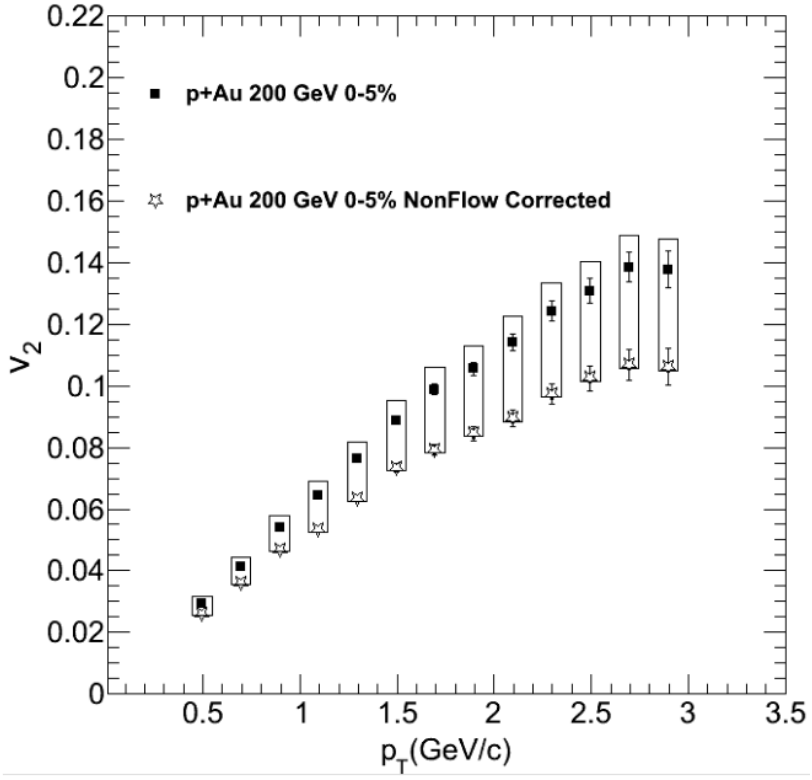

Figure 1.2: The v_2 measurement of p+Au at $\sqrt{s_{NN}}$= 200 GeV $0-5\%$ centrality with the statistical and systematic errors corresponding to the bars and the boxes respectively. The stars are the same p+Aupoints but with the non-flow estimate subtracted rather than treated as a systematic uncertainty. **add ref**

attempt to hold as many variables constant across all three datasets. Table **??** compares the various relevant parameters for the three collision species. Among the differences across the columns, the largest is the lack of non-flow estimates for the d+Audatasets. In the interest of measurement compatibility, and for the reason stated in section .xxx, there is no non-flow correction applied to any of the datasets.

Figure **??** shows the $v_2(p_T)$ measurements in the three systems. All three measurements exhibit substantial v_2 values and rise as a function of p_T with a similar shape. The error bars of each measurement indicate the rough equivalence of the He+Au and d+Au measurements relative to the p+Au measurement. In fact, the systematic error bars are large enough for the p+Au that the difference between p+Au and the other two systems maybe even larger. This effect is especially

Table 1.1: Dataset Variables Comparison listed in order: center of mass energy per nucleon, centrality, mid-rapidity charged particle multiplicity per unit of psuedo-rapidity, year, trigger (as defined in section .xxx) particle sample, trigger particle acceptance, event plane determination, Ψ_2 Resolution, condition of available non-flow estimate, and the eccentricity calculated by Monte Carlo Glauber **add ref**.

Variable	p+Au	d+Au	^{3}He+Au
$\sqrt{s_{NN}}$(GeV)	200	200	200
Centrality	0-5%	0-5%	0-5%
Mid-rapidity $dN_{ch}/d\eta$	N/A	20.8 +/- 1.5	26.3 +/- 1.8
Year (collected)	2015	2008	2014
Trigger Particle Sample	Charged Hadrons	Charged Hadrons	Charged Hadrons
Trigger Particle Acceptance	$\|\eta\| < 0.35$	$\|\eta\| < 0.35$	$\|\eta\| < 0.35$
Event Plane	-3< η <-1 (FVTXs)	-3.7< η <-3.1 (MPCs)	-3< η <-1 (FVTXs)
Ψ_2 Resolution	0.171	0.14	0.274
Non-flow Estimate	yes	no	yes
Glauber ϵ_2	0.23	0.54	0.50

clear at low p_T, where bulk effects would be most dominant. In order to understand the significance of this set of measurements, comparison to standard theoretical models are useful.

1.3 Comparison with Theory

Also shown in Figure **??** are v_2 calculations for each system from the SONIC hydrodynamic model [**?**], which incorporates standard Monte Carlo Glauber initial conditions followed by viscous hydrodynamics with $\eta/s = 0.08$, and a transition to a hadronic cascade at $T = 170$ MeV. More on the SONICE hydrodynamic model is described in greater detail in Chapter 2. It is notable that these calculations for each system are matched to the charged particle density at midrapidity, with the exact values for 0-5% centrality of 10.0, 20.0, and 27.0, for p+Au, d+Au, and He+Au collisions, respectively [**?**]. As mentioned above, the $dN_{cn}/d\eta$ has not been measured for p+Au, and the value of 10.0 was extrapolated from measurements in the other two systems [**?**]. Thus, we see that the calculation includes both the geometry-related change in eccentricity and the relative collision multiplicity. In all cases, a good agreement is seen within the uncertainties between the data and the calculation. These observations strongly support the notion of initial geometry coupled

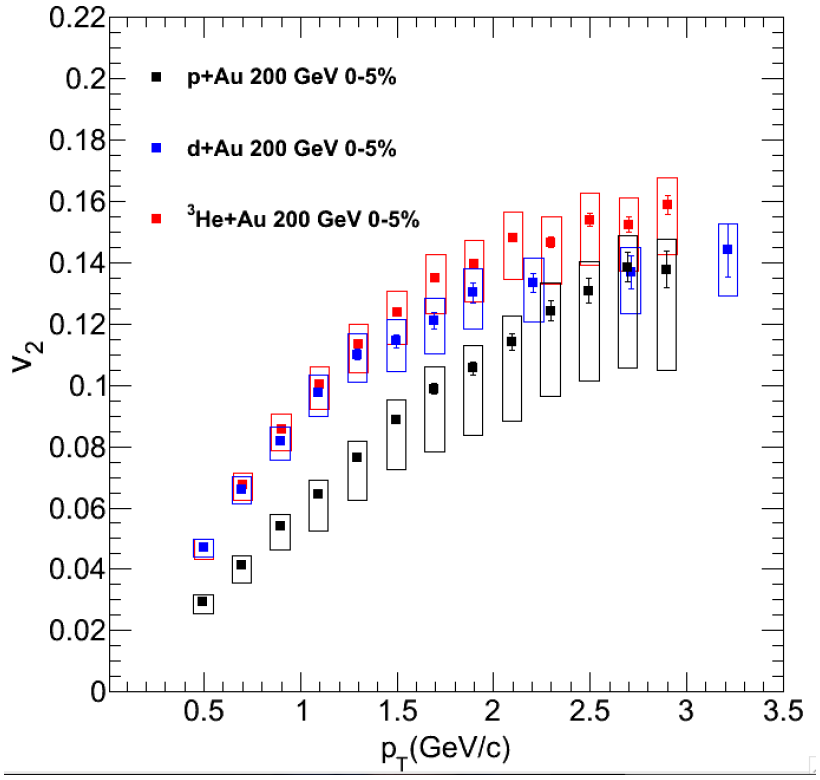

Figure 1.3: v_2 of charged hadrons within $|\eta| < 0.35$ in 0-5% p+Au compared to calculations using the SONIC model match to the same multiplicity as the data. The model calculations have good agreement with the center of the systematic uncertainty bars.

to the hydrodynamic evolution of the medium as a valid framework to understand small system collectivity.

To further explore this idea, we divide the v_2 curves by their corresponding ϵ_2 from Table **??**, attempting to establish a scaling relation between the two quantities. Figure **??** shows that the ratios do not collapse to a common value. As expected, this behavior is also reproduced by the SONIC calculation, because both data and calculation are divided by the same ϵ_2 values. The lack of scaling in the sonic calculation can be understood from d+Au events where the neutron and proton from the deuteron projectile are far separated and create two hot spots upon impacting the Au nucleus, as seen in Figure **??**. These events have a large ϵ_2, but can result in small v_2 if the two hot spots evolve separately, never combining within the hydrodynamic time evolution. This effect

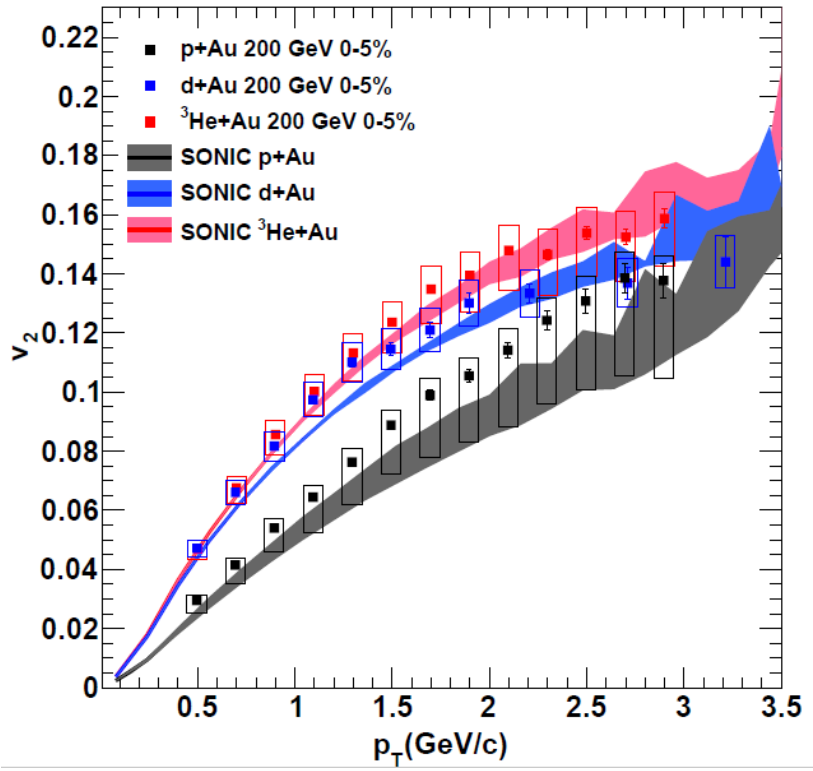

Figure 1.4: v_2 of charged hadrons within $|\eta| < 0.35$ in 0-5% p+Au, d+Au, and He+Au central collisions, compared to hydrodynamic calculations using the SONIC model, matched to the same multiplicity as the data. Note that the data points shown include non-flow contributions, whose estimated magnitude is accounted for in the asymmetric systematic uncertainties.

is present in the d+Au and He+Au systems, and lowers the average v_2/ϵ_2.

1.3.1 Initial Conditions and Eccentricity

In order to better understand the comparison of the three systems, a deeper understand of the initial conditions is warranted.

$$\epsilon_2 = \frac{\sqrt{< r^2 \cos(2\phi) >^2 + < r^2 \sin(2\phi) >^2}}{< r^2 >} \tag{1.1}$$

Figure **??** shows the spatial symmetries present in initial conditions of the three collision species, as well the as a snap shot of the QGP in mid-evolution. Where as the eccentricities of d+Au and He+Au collisions are largely based on relative nucleon orientation, the initial condition of

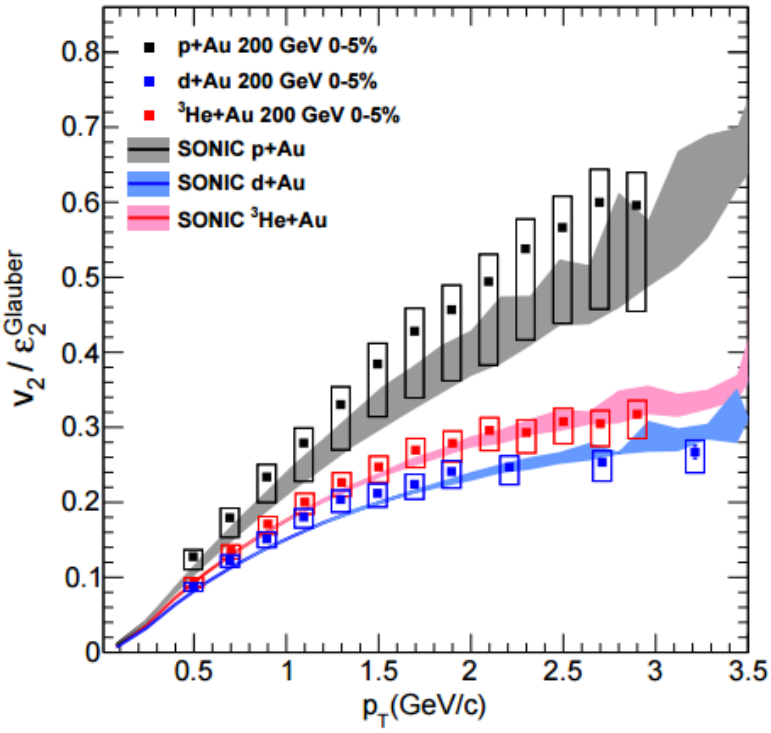

Figure 1.5: v_2 of charged hadrons within $|\eta| < 0.35$ in 05% p+Au, d+Au, and He+Au central collisions, divided by their corresponding eccentricity ϵ_2 from Glauber calculations, compared to sonic calculations of the same quantity. Note that the data points shown include non-flow contributions, whose estimated magnitude is accounted for in the asymmetric systematic uncertainties.

p+Au is solely based on the orientation of the lone proton and any fluctuations in the target gold nucleus. This means that the determination of the eccentricity from d+Au and He+Au is much better understood than that of p+Au, and can give insight into the lack of uniformity in Figure **??**. Table **??** illustrates the uniqueness of the p+Au system by showing the diverging range of ϵ_2 values which can be calculated by different nuclear collision models. In addition to this understanding, the concept of overlapping, expanding hotspots creating substantial final state flow, as seen in section .xxx, shows the relative spatial orientation of the initial hotspots and the symmetry axis of flow, otherwise known as the event plane. For example, in the d+Au collision, the event plane vector is transverse to the line that connects the deuteron's nucleons.

Figure **??** gives an insight into how initial eccentricities, as defined in section xxx., become

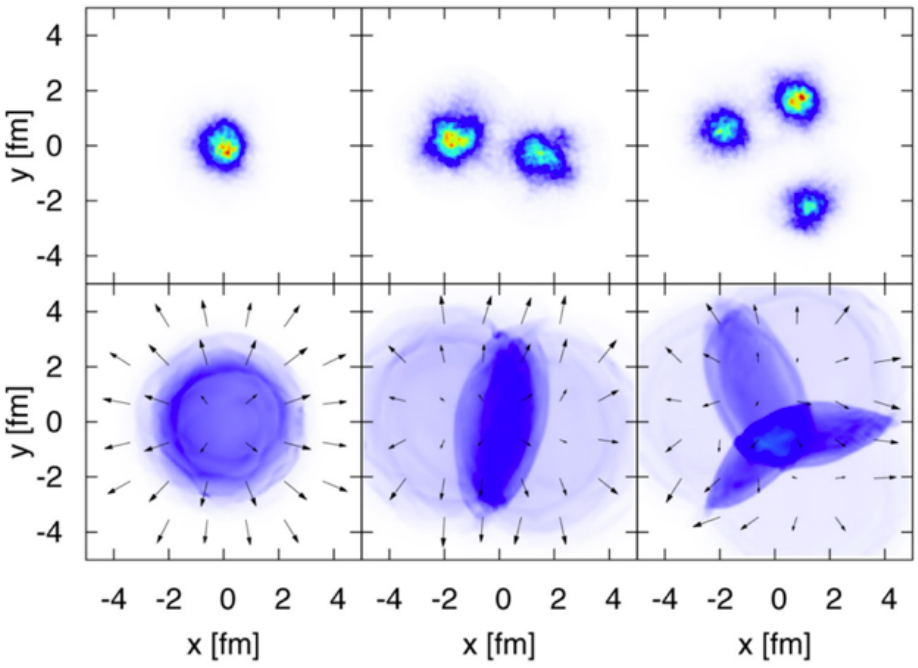

Figure 1.6: The top three panes show the transverse spatial locations of the initial hot spots of the three collision species, p+Au, d+Au, and He+Au respectively as simulated by Monte Carlo Glauber (?). The bottom three plots show the resulting medium produced from the overlapping hot spots as well as the resulting particle momentum vector field as calculated from hydro (?).**add ref**

Table 1.2: Initial eccentricity ϵ_2 of small systems at $\sqrt{s} = 200$ GeV for $0-5\%$ centrality from Monte Carlo Glauber initial conditions smeared with a two-dimensional Gaussian of width $\sigma = 0.4$ fm, and IP-Glasma initial conditions.

	p+Au	d+Au	He+Au
Glauber $\langle\varepsilon_2\rangle$	0.23 ± 0.01	0.54 ± 0.04	0.50 ± 0.02
IP-Glasma $\langle\varepsilon_2\rangle$	0.10 ± 0.02	0.59 ± 0.01	0.55 ± 0.01

transformed into final state flow. The plot was produced by running many events for p+Au, d+Au, and He+Au systems with different values for the shear viscosity and the initial spatial distribution smearing. The final freeze-out hyper-surface of each event is then translated into a distribution of hadrons via the CooperFrye freeze-out prescription **add ref**. In Figure **??**, the flow coefficients from the different systems and the scaling between initial spatial ϵ_2 moments and final

state momentum v_2 values are compared. Figure **??** shows the pion vn at $p_T = 1.0$ GeV/c divided by ϵ_2 as a function of ϵ_2 for each individual p+Au, d+Au, and He+Au event, for different freezeout temperatures $T)F$ controlling the lifetime of the system in the plasma phase. The figure shows a reasonably common scaling of v_2/ϵ_2 for all three systems with the d+Au and He+Au simply extending to larger eccentricities with only a modest dependence on T_F. There are a small set of events with very large ϵ_2, but have a rather small final v_2. Examination of these events reveals them to be d+Au events where the two hot spots are so far apart that the hydrodynamic fluids never connect during the time evolution, as seen in the overlay in Figure **??**, in order to produce nearly any elliptic flow. There are a few He+Au in this category, seen where two nucleons are very close and the third is quite far away, again having the same effect.

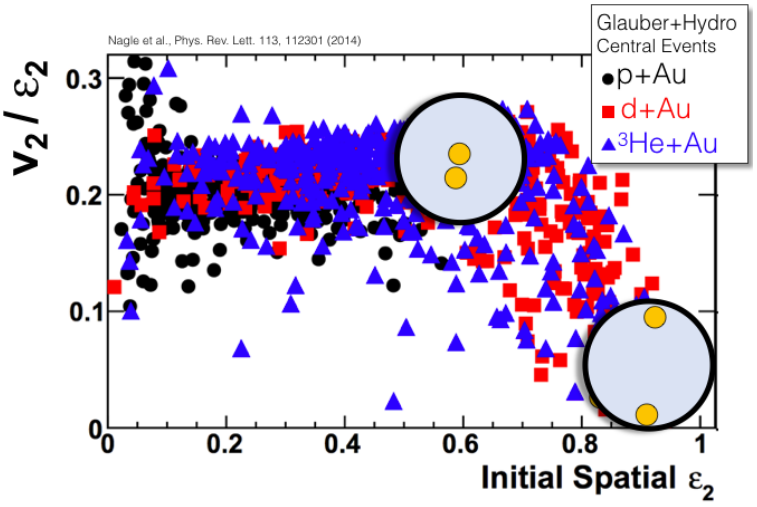

Figure 1.7: v_2/ϵ_2 versus ϵ_2 with the flow coefficient for pions evaluated at $p_T = 1.0$ GeV/c from p+Au, d+au, and He+Au central (b $<$ 2 fm) events. The results are with input parameters $\eta/s = 1/4\pi$ and initial Gaussian smearing $\sigma = 0.4$ fm and a freeze-out temperatures of $T_F = 150$ MeV. Diagrams of two possible d+Au initial configurations are overlayed on top of the plot. Increasing distance between the two d+Au nucleons correspond to a larger ϵ_2.**add ref**

Another model that incorporates degrees of freedom extends the Monte Carlo Glauber approach to also incorporate collisions between constituent quarks . Recently, this framework has been successfully applied to the description of midrapidity charged particle multiplicity and trans-

verse energy production **add ref**. Different implementations of constituent quark Monte Carlo Glauber calculations are detailed in **add refs**. In Figure 13(f) of Ref. [12], the initial eccentricities ϵ_2 in p+Au, d+Au, and He+Au obtained by incorporating constituent quarks, in addition to multiplicity fluctuations, are found to be $\epsilon_2 = 0.42$, 0.54, and 0.54, respectively. This calculation assumes a Gaussian density distribution of low-x gluons around each constituent quark, of width $\sigma_g = 0.3$ fm. It is interesting to note that the d+Au and He+Au systems show little sensitivity to the incorporation of both constituent quarks and multiplicity fluctuations into the calculation of the initial ϵ_2. Conversely, under the same circumstances, p+Au has a substantially larger ϵ_2 than in the models shown in Table **??**. Ref. [13] also presents calculations incorporating nucleonic degrees of freedom and multiplicity fluctuations, in which case a lower $\epsilon_2 = 0.34$ is obtained for p+Au. This shows that, when compared to the Glauber ϵ_2 for p+Au in Table **??**, quark-level degrees of freedom and multiplicity fluctuations may both play a significant role.

1.3.2 Comparison to Alternative Models

Although hydrodynamic models like SONIC are the standard in which elliptical flow is understood in the field of heavy ions, it is important to test the accuracy and consistency of other models against our data. Figure **??** depicts the established $v_2(p_T)$ data curves with four different model comparisons. Theoretical predictions are available in the literature, most notably from hydrodynamics with Glauber initial conditions (SONIC **add ref** and SUPERSONIC **add ref**), hydrodynamics with IP-Glasma initial conditions **add ref**, and A-Multi-Phase-Transport Model (AMPT) **add ref**. The SUPERSONIC model uses the same prescription for initial conditions, hydrodynamic expansion, and hadronic cascade as SONIC, yet additionally incorporates pre-equilibrium dynamics with a calculation in the framework of the AdS/CFT correspondence **add ref**.

For the model of IPGlasma+Hydro, in the case of d+Au and He+Au, a better agreement with data can be achieved by increasing the value of η/s or by including a hadronic cascade stage. However, doing so would lower the prediction for p+Au even further. This demonstrates that IP-Glasma does not generate the appropriate initial conditions to account for measured v_2 via

hydrodynamic flow.

SONIC and SUPERSONIC agree well with the data within uncertainties, supporting the idea of initial geometry as the driver of the v_2 signal. Furthermore, this illustrates how these results impose useful constraints to reduce the number of free parameters of the model, because many such parameters must be identical across systems, e.g., η/s, the transition temperature to a hadron cascade, and the Monte Carlo Glauber smearing of nucleon coordinates of $\sigma = 0.4$ fm.

Calculations using IP-Glasma initial conditions followed by viscous hydrodynamics have been successfully used to describe collectivity in A+A collisions **add ref**. It is notable that in these calculations the glasma framework is used only to determine the initial spatial configuration as input to hydrodynamics; there is no glasma diagram or momentum domain physics incorporated, such that all of the collectivity arises from final-state interactions. When this framework is applied to small collision systems with η/s = 0.12 and b $<$ 2 fm, as shown in Figure **??**, the calculation substantially overestimates the data for d+Au and He+Au, while underestimating it for p+Au. This follows from the fact that IP-Glasma generates very circular initial conditions for p+Au, corresponding to very low ϵ_2 values; however, the presence of several hot spots in d+Au and He+Au result in IP-Glasma values for ϵ_2 more comparable to those from Glauber. This is shown in Table **??**.

It is important to notice that additional degrees of freedom for the geometry of p+Au collisions arise from fluctuations of the shape of the proton, as described in Ref. **add ref**. The contribution of this effect to the measured elliptic flow may be constrained by p+p data, and also possibly by varying the target in other p+A systems.

Finally, AMPT, as described in Chapter 2, combines partonic and hadronic scattering in a single model. Central AMPT events with impact parameter $b < 2$ have a midrapidity $dN_{ch}/d\eta =$ 8.1, 14.8, and 20.7 for p+Au, d+Au, and He+Au, respectively. These were generated with the same Monte Carlo Glauber initial conditions used to characterize event geometry, and thus have very similar eccentricities to those given in Table **??**. Using the initial Glauber geometry information to compute v_2 relative to the participant plane [**?**] yields results that agree reasonably well with the

data below $p_T \approx 1$ GeV/c, yet under predict them at higher p_T. It is noteworthy that despite the very different physics of AMPT compared to the other models, it has successfully been applied to a variety of systems at RHIC and the LHC **add refs**.

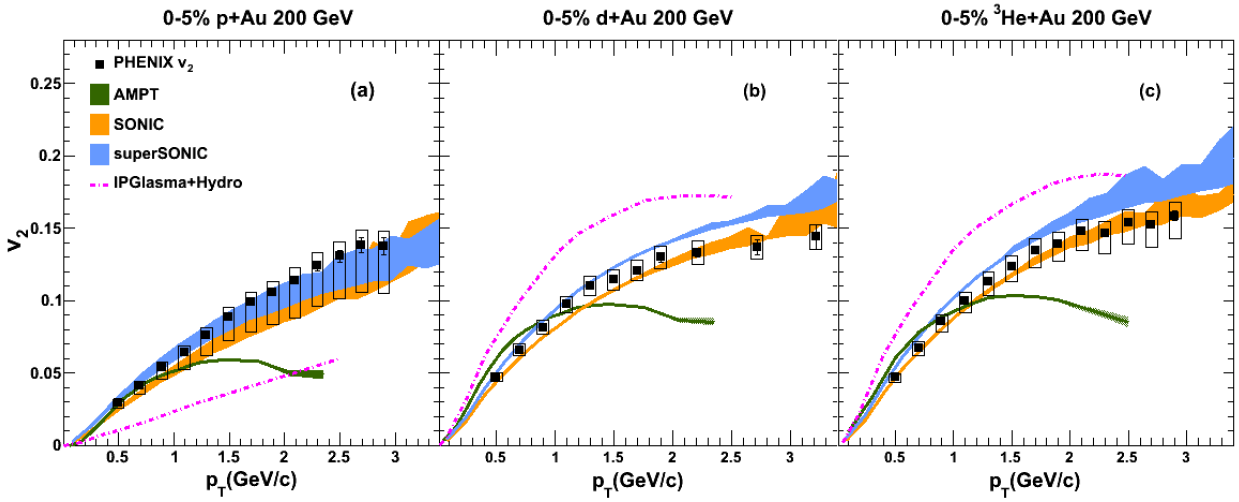

Figure 1.8: Transverse momentum dependence of v_2 in central 0-5% (a) p+Au, (b) d+Au, and (c) He+Au collisions at $\sqrt{s_{NN}}$= 200 GeV. Theoretical calculations from AMPT, SUPERSONIC, and IPGlasma+Hydro are shown in each panel. Note that the data points shown include non-flow contributions, whose estimated magnitude is accounted for in the asymmetric systematic uncertainties.

These results impose strong constraints on any model attempting to describe small system collectivity, whether by the formation of strongly interacting hot nuclear matter, or by other mechanisms. We observe an imperfect scaling of v_2 with ϵ_2, well reproduced by hydrodynamics, providing strong evidence for initial geometry as the source of final-state momentum anisotropy in these systems. This disfavors other explanations based on initial-state momentum space domain effects.

Bibliography

[1] Event reconstruction in the {PHENIX} central arm spectrometers. Nucl.Instrum.Meth, A482:491–512, 2002.

[2] Rhic operations with asymmetric collisions in 2015. 2015.

[3] A. et al Adare. Measurements of elliptic and triangular flow in high-multiplicity ^{3}He + Au collisions at $\sqrt{s_{NN}} = 200$ GeV. Phys. Rev. Lett., 115:142301, Sep 2015.

[4] S. S. et al Adler. Absence of suppression in particle production at large transverse momentum in $\sqrt{s_{NN}} = 200$ GeV d + Au collisions. Phys. Rev. Lett., 91:072303, Aug 2003.

[5] J. et al Beringer. Review of particle physics. Phys. Rev. D, 86:010001, Jul 2012.

[6] Siegfried Bethke. The 2009 world average of α. The European Physical Journal C, 64(4):689–703, 2009.

[7] C. Aidala et al. The {PHENIX} forward silicon vertex detector. Nuclear Instruments and Methods in Physics Research Section A: Accelerators, Spectrometers, Detectors and Associated Equipment, 755:44 – 61, 2014.

[8] K. Adcox et al. {PHENIX} detector overview. Nuclear Instruments and Methods in Physics Research Section A: Accelerators, Spectrometers, Detectors and Associated Equipment, 499(2?3):469 – 479, 2003. The Relativistic Heavy Ion Collider Project: {RHIC} and its Detectors.

[9] A Fedotov. Progress of high-energy electron cooling for rhic.

[10] Enrico Fermi. High energy nuclear events. Progress of Theoretical Physics, 5(4):570–583, 1950.

[11] Charles Gale, Sangyong Jeon, Björn Schenke, Prithwish Tribedy, and Raju Venugopalan. Event-by-event anisotropic flow in heavy-ion collisions from combined yang-mills and viscous fluid dynamics. Phys. Rev. Lett., 110:012302, Jan 2013.

[12] M. Habich, J. L. Nagle, and P. Romatschke. Particle spectra and hbt radii for simulated central nuclear collisions of c+c, al+al, cu+cu, au+au, and pb+pb from sqrt(s)=62.4-2760 gev. The European Physical Journal C, 75(1):15, 2015.

[13] A. M. Poskanzer and S. A. Voloshin. Methods for analyzing anisotropic flow in relativistic nuclear collisions. Phys. Rev. C, 58:1671–1678, Sep 1998.

[14] Johann Rafelski. Connecting qgp-heavy ion physics to the early universe. Nuclear Physics B - Proceedings Supplements, 243:155 – 162, 2013.

[15] T. Roser. Rhic performance. Nuclear Physics A, 698(1):23 – 28, 2002.

[16] XIAO-MING XU. ORIGIN OF TEMPERATURE OF QUARK-GLUON PLASMA IN HEAVY ION COLLISIONS, pages 203–208. WORLD SCIENTIFIC, 2015.